*Desalination and Water Treatment*
www.deswater.com

doi: 10.5004/dwt.2019.24596

167 (2019) 258–268
November

# Treatment of molybdenum(VI)-containing groundwater using chitosan nanoparticle: adsorption mechanism and performances

Jian-jun Lian[a,b], Mei Yang[a,b], Shi-sheng Wang[a,b], Bo Chen[a,b,*], Fan-jie Zhou[a,b], Zai-liang Liu[a,b]

[a]*College of Energy and Environment, Anhui University of Technology, Anhui 243002, China, emails: greenchenbo@163.com (B. Chen), jjlian85@126.com (J.-j. Lian), 15755505979@163.com (M. Yang), ahutsswang@163.com (S.-s. Wang), 18395565216@163.com (F.-j. Zhou), liuzailiang2008@163.com (Z.-l. Liu)*
[b]*Water Purification by Biofilm Method and Utilization, Engineering Research Center of Ministry of Education, Anhui University of Technology, Anhui 243032, China*

Received 19 December 2018; Accepted 18 June 2019

**ABSTRACT**

A novel nano-adsorbent prepared by hydrothermal carbonization of chitosan was used for removing molybdenum (Mo(VI)) from groundwater. Optimal adsorption parameters were determined via varying pH, time, concentrations, and temperatures. The results indicated that the removal rate of Mo(VI) by chitosan carbonization nanoparticles (CCN) was depended on pH values and the maximum adsorption efficiency could be achieved when the pH is in the range of 1.5–3.3. Kinetic studies showed that Mo(VI) could be removed rapidly, and the experimental results fitted pseudo-second-order kinetic model well. Mo(VI) adsorbed by CCN was described well by Langmuir model and the theoretical maximum adsorption capacity reached 192.308 mg $g^{-1}$ at 303.15 K. Thermodynamic parameters indicated that the adsorption process was endothermic, entropy increasing, and spontaneous. Electrostatic interaction and hydrogen bonding were the major adsorption mechanisms. Regeneration and real groundwater treatment experiments revealed that Mo(VI) could be removed efficiently by CCN, and CCN could be recycled for a long term. Altogether, CCN might be a green, efficient, and recyclable adsorbent for Mo(VI) removal from groundwater.

*Keywords:* Molybdenum; Adsorption; Chitosan carbonization nanoparticles; Groundwater; Mechanism

## 1. Introduction

Molybdenum (Mo) is not only an essential micronutrient for both plants and animals but also a very important strategic resource [1,2]. The provisional daily intake of Mo recommended is 75–250 μg for adolescent boys and girls [3]. Nevertheless, water-soluble Mo will cause environmental pollution if its concentration exceeds 5 mg $L^{-1}$, in addition, the toxic degree ranks between those of Zn(II) and Cr(III) compounds [4]. Notably, Mo pollution in groundwater has been deemed as a serious issue in some fields of drinking water obtained from wells [5]. For example, Mo concentrations varied from a few mg $L^{-1}$ to 800 mg $L^{-1}$ in some mill tailings of North America [6]. Moreover, Mo pollution events have been reported in some other places, such as in Brenda Mines of British Columbia, Canada; the San Joaquin Valley, USA; and Wujintang Reservoir, China [7,8], which can also pollute groundwater through various ways such as rainfall runoff. However, there are few reports about the removal of Mo pollution from groundwater.

Mo can exist in various oxidation states ranging from +2 to +6 in water, while $MoO_4^{2-}$ is the most soluble form

* Corresponding author.

among Mo compounds, and it is widely distributed in natural environment and water bodies [8]. Methods, for example, chemical precipitation [9] and ion-exchange [10] have been developed for Mo pollution control in surface water, but the cost is too high for the various reagents and complicated instruments. Adsorption gained wide acceptance because it is an efficient and economically feasible process for purification [11]. Numerous materials including chelating resin [12], pyrite [13], desulfurization steel slag [14], nano-magnetic $CuFe_2O_4$ [15], ocetylpyridinium bromide-bentonite [16] have been reported for the adsorption of Mo(VI), which indicated that protonated materials are conducive to Mo(VI) removal.

Chitosan (CS), an abundant natural polysaccharide, with a large amount of free amino and hydroxyl functional groups on its structure, is considered as an excellent adsorbent for the treatment of organic anions (methyl orange, methylene blue, dyes) and heavy metal cations (Cr(VI), Cu(II), Cd(II), Zn(II), as well as Pb(II)) [17–19]. Therefore, it is reasonable to deduce that CS is also likely suitable for the removal of Mo from groundwater. However, raw chitosan is water soluble at pH < 6.0 which limited its application as adsorbent [20]. Some modified CS adsorbents such as magnetic chitosan nanoparticle [21], molybdate-imprinted chitosan/triethanolamine gel beads [22] have been developed for Mo(VI) removal, but the preparation process is too complex.

The objective of this paper was to remove Mo(VI) by a new chitosan carbonization nanoparticle (CCN) adsorbent. To our best knowledge, no other studies employing CCN for treatment of Mo(VI) contaminated groundwater have been reported. The effects of pH, temperature, adsorption kinetics, adsorption isotherms, and adsorption mechanism were particularly investigated. Regeneration tests and actual groundwater experiments were also studied in order to illustrate the practicality of Mo(VI) removal by CCN. The results of this study not only expand the application range of chitosan, but also provide reference for Mo(VI)-containing groundwater treatment technology.

## 2. Materials and methods

### 2.1. Materials and chemicals

Sodium molybdate 2-hydrate ($Na_2MoO_4{\cdot}2H_2O$) was employed to prepare a stock solution containing 1,000 mg $L^{-1}$ of Mo(VI). 80%–95% deacetylated chitosan powders were supplied by Sinopharm Chemical Reagent Co. Ltd., China. All other chemicals were of analytical grade and commercially available from Shanghai Chemical Reagent Co. Ltd. and used without further purification. Milli-Q water was used to prepare aqueous solutions.

### 2.2. Synthesis of the CCN

First, 4.0 g of CS was dispersed in 75 mL Milli-Q water by ultrasonic to obtain a homogeneous dispersion at room temperature. Then, the mixed solution was transferred into a 100 mL teflon-lined stainless steel autoclave. Finally, the container was closed and maintained at 180°C for 12 h. After that, the autoclave was cooled to room temperature naturally. Then, the as-prepared nanocomposite (CCN) was obtained by filtering, rinsing, drying, grinding, and sieving (<0.15 mm) prior to use.

### 2.3. Batch adsorption experiments

Batch adsorption experiments were carried out by agitating 0.1 g of CCN with 100 mL aqueous solution contained different Mo(VI) concentration in a constant temperature oscillator with speed of 150 rpm. The ionic strength of the Mo(VI) solution adjusted by NaCl was controlled at 0.1 mol $L^{-1}$. All the experiments were conducted with three parallel tests. The data presented in all tables and figures are average values.

The adsorption kinetics experiment were carried out with initial Mo(VI) concentration of 50, 100, and 200 mg $L^{-1}$ for different time intervals at an optimum pH. Adsorption isotherm studies were performed with Mo(VI) concentrations ranging from 5 to 500 mg $L^{-1}$ at 10°C, 20°C, and 30°C. When the adsorption of Mo(VI) by CCN reached equilibration, the suspensions were filtered through 0.45 μm filters for further analyzing the residual Mo.

The effect of pH on the adsorption performance of Mo(VI) was conducted by adding 0.1 g of CCN into 100 mL of 10 mg $L^{-1}$ Mo(VI) aqueous solution under different pH value. The solution pH was adjusted to 1.0–10.0 using 1 mol $L^{-1}$ HCl or NaOH, and the changed total volume was <2%. After adding 0.1 g of CCN, all the samples were shaken for 24 h at 20°C, then the residual Mo concentration was measured. The point of zero charge (pzc) of the material was determined as described in literature [23].

### 2.4. Regeneration

In order to evaluate the regeneration ability of CCN, the adsorption and desorption tests of Mo(VI) was studied for consecutive five cycles. In each cycle, CCN was added into 50 mg $L^{-1}$ of the Mo(VI) solution with adsobent dosage of 5.0 g $L^{-1}$ and the mixture was shaken in a shaker with speed of 150 rpm for 8 h. After that, the Mo(VI)-adsorbed CCN was separated from the solution by centrifugation and then using 40 mL of 0.1 mol $L^{-1}$ NaOH for Mo(VI) desorption by shaking for 1 h. After desorption, the CCN was collected and the amount of desorbed Mo(VI) in aqueous solution was examined. After each cycle of regeneration experiments, CCN was washed and dried overnight for the next cycle.

### 2.5. Real groundwater treatment

Groundwater was collected from a tube well nearby a molybdenum ore in Xinzhou City, China. The groundwater quality parameters (mg $L^{-1}$) were analyzed by standard methods [24], which contained total hardness (1,350.24), sulfate (1,239.04), nitrate (14.13), nitrite (4.87), ammonia (0.64), organic matter (1.46), iron (0.11), manganese (0.07), total arsenic (0.01), copper (0.87), zinc (0.55), total chromium (0.03), Mo(VI) (0.23), and pH (6.75). This groundwater sample was spiked with Mo(VI) up to a level of desire (10.0 mg $L^{-1}$) for further experiments, the pH and reaction time were adjusted to the optimum value according to the above analysis.

### 2.6. Analysis

The structure and surface characteristics of adsorbents were measured using scanning electron microscopy (SEM; FEI Quanta 200). Powder XRD patterns at two angles from

10° to 80° were recorded at an interval of 0.33° on a UItima IV diffractometer using Cu radiation (40 kV, 40 mA). FTIR spectra were recorded on a Nicolet 6700 FTIR spectrophotometer. The XPS analysis was taken by an X-ray photoelectron spectroscopy Escalab 250Xi with the monochromatic Al K$\alpha$ X-ray radiation. The pH value of the solution was measured by S-3C model pH meter, while the concentrations of Mo were determined by thiocyanate photometric method [25].

## 3. Results and discussion

### 3.1. Adsorbent characterization

Typical field-emission scanning electron microscopy images of the CCN and CCN-Mo are shown in Fig. 1. In general, CCN (100,000×) has near-spherical shape, and its diameter is less than 50 nm (Fig. 1a). As for CCN-Mo (100,000×) (Fig. 1b), a similar shape is observed compared with original CCN surface with exception of a larger diameter (>50 nm). Moreover, compared with the surface of CCN-Mo (20,000×) (Fig. 1d), the particles of CCN (20,000×) (Fig. 1c) are clearer and more evenly distributed, which further confirms that Mo was successfully adhered to the external structure of CCN by the adsorption process.

The crystalline structure of the CCN and CCN-Mo was studied by XRD and the diffractograms are shown in Fig. 2. It can be seen from XRD patterns, adsorption of Mo sharply decreased the crystalline nature of CCN. CCN showed obvious diffraction peak at 20° corresponding to its crystalline phase [19,26]. However, after adsorbed Mo, the peak of CCN-Mo has been significantly weakened and shifted. It indicated that introduction of Mo in the CCN matrix disrupts its crystalline structure, especially by loss of the hydrogen bonding.

### 3.2. Mo(VI) adsorption process

#### 3.2.1. Effect of pH

The pH value can affect the metal species in solution and the surface properties of the adsorbents, so it is an important influencing parameter for adsorption of metal ions in water [27]. As shown in Fig. 3, it is evident that Mo(VI) adsorption onto CCN were highly pH-dependent. The maximum Mo(VI) adsorbed by CCN occurs when the pH value in the range of 1.5–3.3. The maximum Mo(VI) removal may be due to the surface protonation of the sorbent and the change of Mo(VI) to other species. The $pH_{zpc}$ of the CCN is 3.9. However, the speciation of Mo anions are anionic polynuclear hydrolyzed species within pH in the range of 2.0–4.6 [28]. Therefore, the adsorbent surface is positively charged when pH is below the $pH_{zpc}$, and anion adsorption occurs. The decrease in the

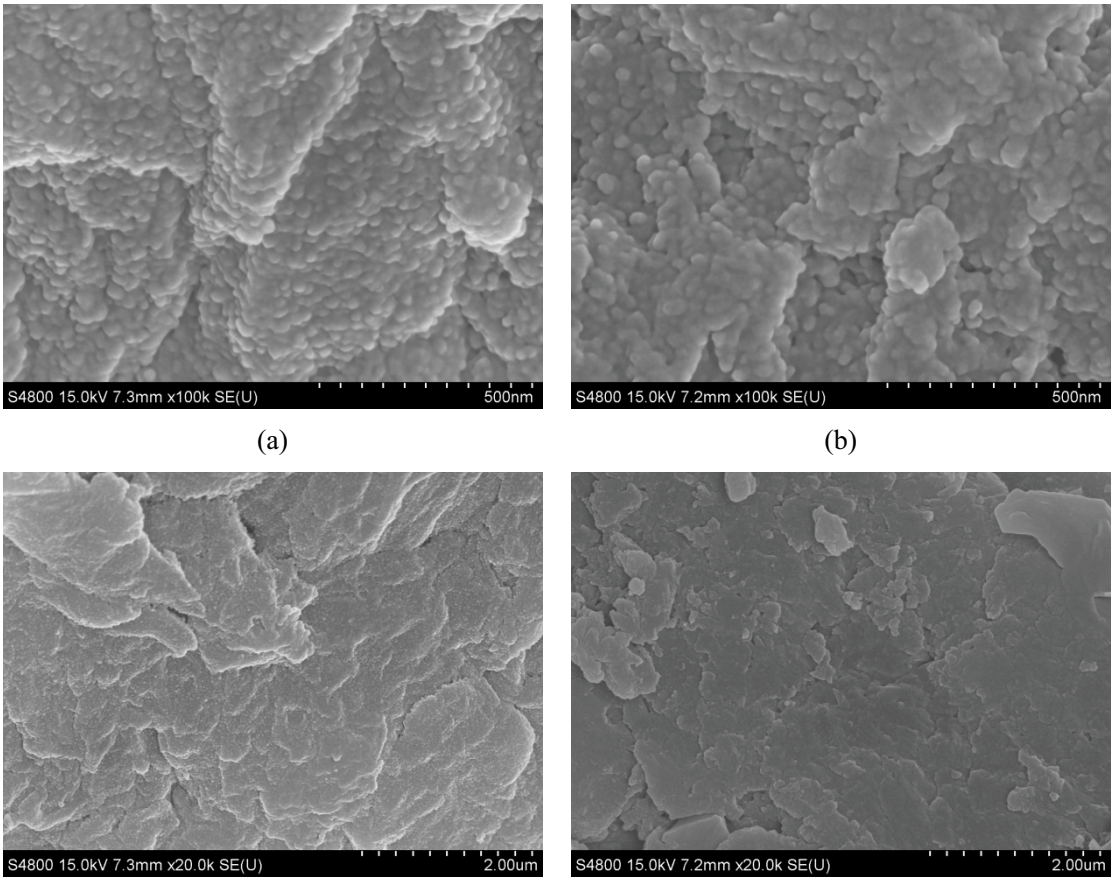


Fig. 1. Surface appearance of (a) CCN (100,000×), (b) CCN-Mo (100,000×), (c) CCN (20,000×), and (d) CCN-Mo (20,000×).

removal at pH > 4.0 is due to the weakening of the surface protonation. When the pH value is increased to 8.0, the percentage of Mo(VI) adsorption decreased rapidly toward a negligible level by the end of the test (<20%). It is noted that electrostatic attraction played an important role in Mo(VI) adsorption on CCN.

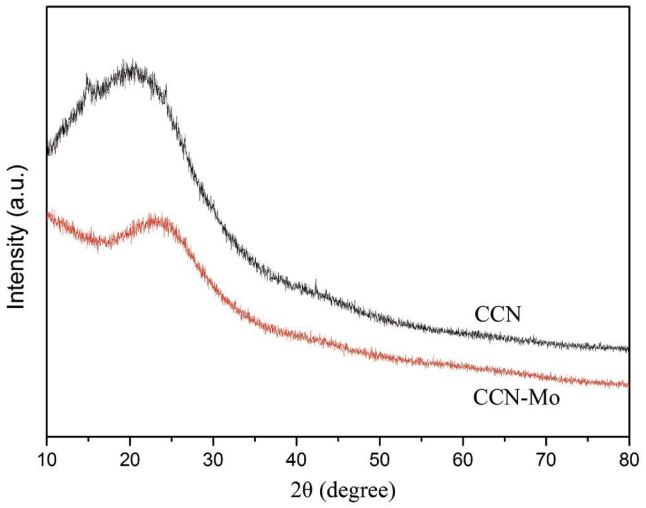


Fig. 2. XRD spectra of the CCN and CCN-Mo.

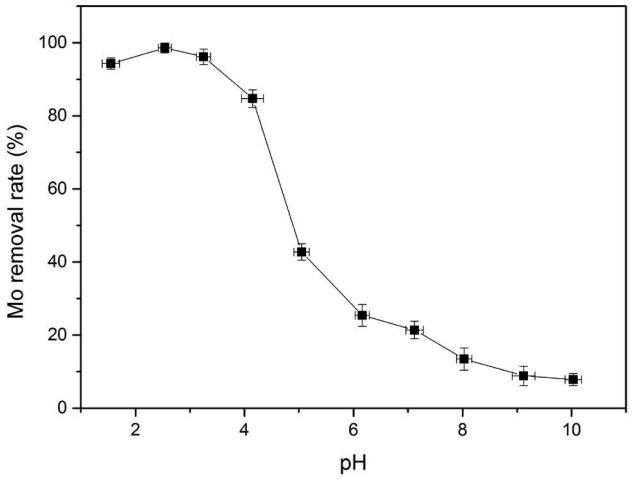


Fig. 3. Effect of initial pH values on Mo(VI) adsorption by CCN. Conditions: CCN dosage = 1.0 g $L^{-1}$, $T$ = 293.15 K, initial Mo concentration = 10 mg $L^{-1}$.

*3.2.2. Adsorption kinetic studies*

The adsorption kinetics of Mo(VI) by CCN was investigated with reaction time ranging from 0 to 900 min at pH 2.5, 293.15 K. The initial Mo(VI) concentrations were 50, 100 and 200 mg $g^{-1}$, respectively. Fig. 4a shows that adsorption capacity of CCN increased with the increasing of time until it reached equilibrium under different Mo(VI) concentration. Besides, the adsorption performance of CCN with respect to Mo(VI) was rapid initially and then slowed down gradually until it attained equilibrium. In the initial stage, there are a large number of vacant surface sites for Mo(VI) adsorption. As reaction time was prolonged, the remaining vacant surface sites are difficult to be occupied for steric hindrance between Mo(VI) adsorbed on the surface of CCN and solution phase. In order to better investigate the adsorption mechanism of Mo(VI) onto CCN, the pseudo-first-order kinetic model and pseudo-second-order kinetic model were adopted to interpret data obtained from batch experiments according to the two equations that have been expressed in our previous work [14].

The correlative parameters calculated by the pseudo-first-order kinetic model and pseudo-second-order kinetic model are presented in Table 1 and the fitting results of the two kinetic models are shown in Figs. 4b and c. The results showed that the calculated values ($q_{e,cal,2}$) obtained from the pseudo-second-order kinetic model are very close to the experimental value ($q_{e,exp}$). Moreover, the correlation coefficients ($R^2$) of the pseudo-second-order kinetic equation is relatively greater than that of pseudo-first-order kinetic model, suggesting that pseudo-second-order kinetic model is more suitable for describing Mo(VI) adsorption onto CCN based on the assumption that the rate-limiting step may be chemisorption involving valence forces through sharing or exchanging electrons between adsorbate and adsorbent [29].

Solute adsorption onto the solid surface can be controlled by several steps, for example, external diffusion, surface diffusion, and pore diffusion [30]. In order to confirm the actual rate-controlling step in the Mo(VI) adsorption process, the well-known Weber–Morris equation was applied [31]:

$$q_t = k_i t^{0.5} + I \quad (1)$$

where $q_t$ (mg $g^{-1}$) is the amounts of metal ion adsorbed onto adsorbent at time $t$ (min), $k_i$ is intraparticle diffusion rate (g $mg^{-1}$ $min^{-0.5}$), $I$ represents the boundary layer diffusion constants (external film resistance). The plots of $q_t$ against $t^{0.5}$ give straight line with slope and intercept equal $k_i$ and $I$, respectively. If the plots of $q_t$ vs. $t^{0.5}$ satisfy the linear relationship and pass through the origin, the adsorption process

Table 1
Kinetic parameters of pseudo-first-order and pseudo-second-order for Mo(VI) adsorbed by CCN

| $C_0$ (mg $L^{-1}$) | $q_{e,exp}$ (mg $g^{-1}$) | Pseudo-first-order | | | Pseudo-second-order | | |
|---|---|---|---|---|---|---|---|
| | | $q_{e,cal,1}$ (mg $g^{-1}$) | $k_1$ (1 $min^{-1}$) | $R^2$ | $q_{e,cal,2}$ (mg $g^{-1}$) | $k_2$ (mg (g $min)^{-1}$) | $R^2$ |
| 50 | 47.104 | 10.102 | 0.0030 | 0.8126 | 49.020 | 0.0027 | 0.9999 |
| 100 | 88.649 | 18.754 | 0.0032 | 0.8337 | 93.458 | 0.0014 | 0.9999 |
| 200 | 143.025 | 52.857 | 0.0041 | 0.9104 | 147.059 | 0.0004 | 0.9995 |

should be controlled by internal diffusion. Otherwise, more steps may influence the adsorption process.

The plots of $q_t$ vs. $t^{0.5}$ are given in Fig. 4d for the adsorption of Mo(VI) by CCN at different initial Mo(VI) concentrations. Obviously, the adsorption data were well-fitted by two straight lines, indicating that two steps took place during Mo(VI) adsorption onto CCN. First, Mo(VI) in aqueous solution was transported onto the surface of CCN, then Mo(VI) was transported and adsorbed on the interior surface of CCN [32]. Besides, the time in intraparticle diffusion state is longer than that of external diffusion state in Fig. 4d, indicating that the intraparticle diffusion is the main rate-controlling state. The detailed fitting model parameters is shown in Table 2. The $R^2$ values are close to unity, confirming the applicability of Weber–Morris model for Mo(VI) adsorption on CCN. The constant $I_2$ values increased with the increasing of Mo(VI) concentration of Mo(VI), suggesting that the boundary layer thickness was increased with increasing initial Mo(VI) concentration.

### 3.2.3. Adsorption isotherm studies

The adsorption isotherm will reflect the specific relation between the concentration and accumulation degree of

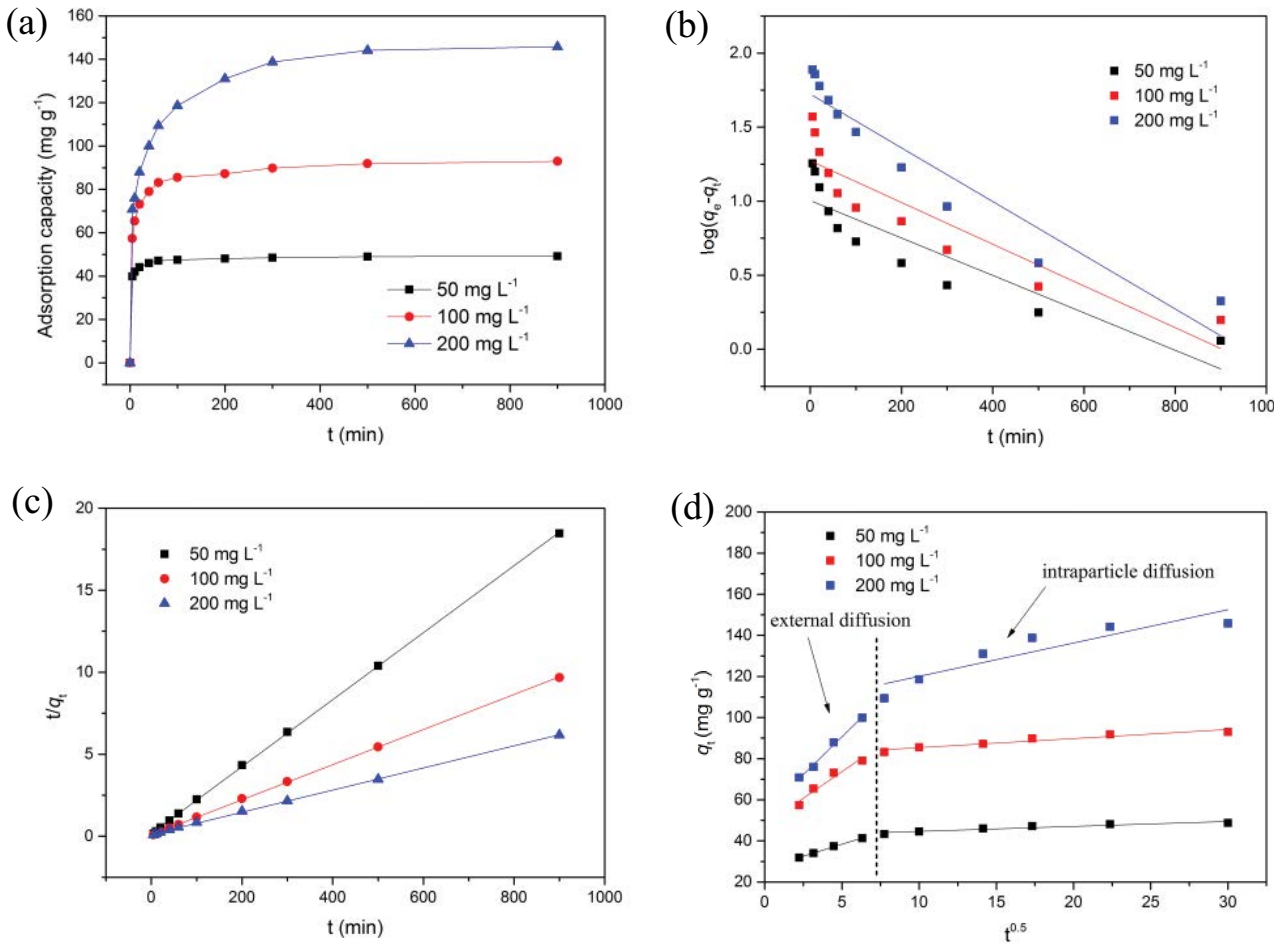


Fig. 4. Effect of contact time for the adsorption of Mo(VI) onto CCN (a), and linear fitting of pseudo-first-order kinetic model (b), pseudo-second-order kinetic model (c), and Weber–Morris diffusion model (d). Conditions: CCN dosage = 1.0 g $L^{-1}$, T = 293.15 K and pH = 2.5.

Table 2
Kinetic parameters of Weber–Morris model for Mo(VI) adsorption on CCN

| $C_0$ (mg $L^{-1}$) | First stage | | | Second stage | | |
|---|---|---|---|---|---|---|
| | $I_1$ | $k_{i,1}$ (mg $g^{-1}$ $min^{-0.5}$) | $R^2$ | $I_2$ | $k_{i,2}$ (mg $g^{-1}$ $min^{-0.5}$) | $R^2$ |
| 50 | 26.688 | 2.3367 | 0.9974 | 42.208 | 0.2419 | 0.9018 |
| 100 | 47.792 | 5.174 | 0.9531 | 80.965 | 0.4408 | 0.9228 |
| 200 | 53.97 | 7.3293 | 0.9938 | 103.84 | 1.622 | 0.9005 |

adsorbate onto the adsorbent surface at a constant temperature. Herein, the adsorption isotherms of Mo(VI) adsorbed by CCN were investigated at different initial Mo(VI) concentrations within temperature in the range of 283.15–303.15 K when the pH value was 2.5. As shown in Fig. 5, the adsorption capacities ($q_e$) were increased quickly at low $C_e$ values, whereas the increment of $q_e$ was slowed down at higher values of $C_e$, which is due to the limited active sites on the surface of CCN for relatively high Mo(VI) concentration. Besides, the amount of adsorbed Mo(VI) by CCN increased as temperature increased, implying that the adsorption process was endothermic.

In order to gain a better understanding of adsorption performance for Mo(VI) adsorbed by CCN, four isotherm models including Langmuir isotherm, Freundlich isotherm, Temkin isotherm, and Dubinin–Radushkevich isotherm have been used to fit the experimental data [14]. The adsorption plots and the fitting model parameters with $R^2$ for the different models are separately shown in Fig. 6 and Table 3.

The $R^2$ values of Langmuir isotherm model are higher than that obtained from other three isotherms (Table 3). It may be due to the homogeneous distribution of active sites on the adsorbent surface. A comparison of Mo(VI) adsorption capacity of some adsorbents based on the values of $Q_0$ (Table 4) is comparable with the results obtained in previous studies. It was found that CCN had a higher adsorption capacity in comparison with the reported adsorbents, indicating CCN can be used as an alternative material for Mo(VI) removal from solution. From the Temkin isotherms, typical bonding energy range for the ion exchange mechanism was reported to be in the range of 8–16 kJ mol$^{-1}$,

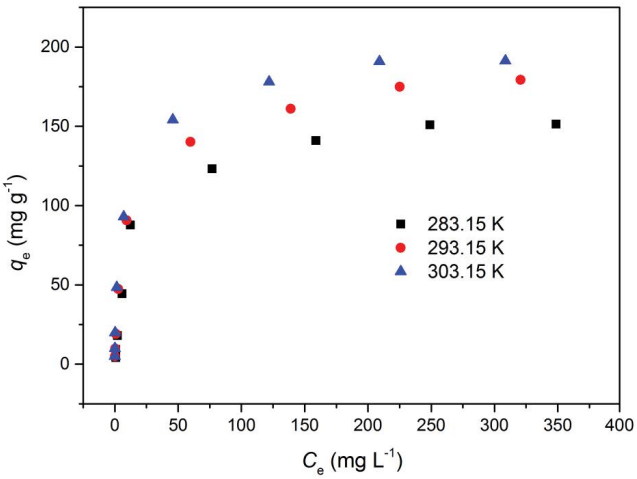


Fig. 5. Adsorption isotherms data for Mo(VI) on CCN. Conditions: CCN dosage = 1.0 g L$^{-1}$, pH = 2.5.

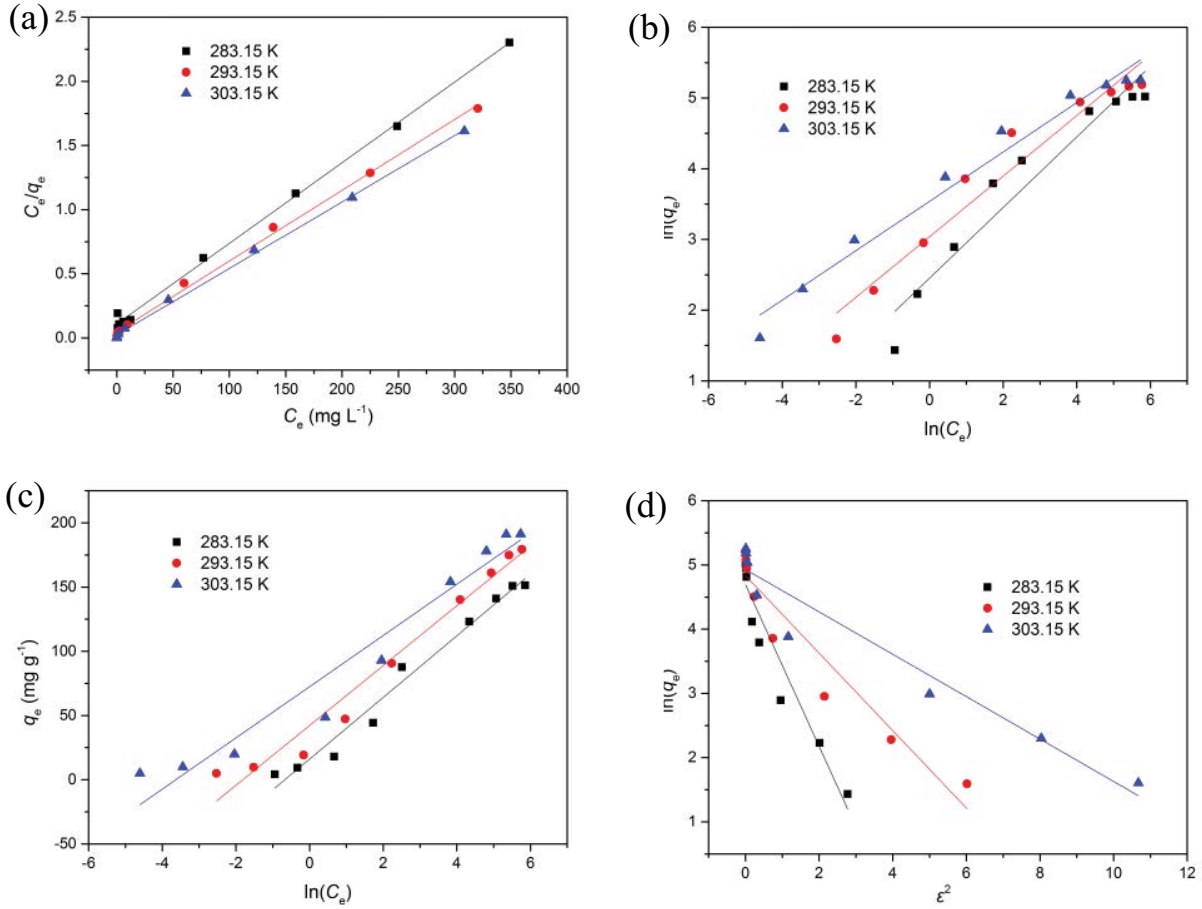


Fig. 6. Adsorption isotherms data and modeling for Mo(VI) on CCN. (a) Langmuir isotherm, (b) Freundlich isotherm, (c) Temkin isotherm, and (d) Dubinin–Radushkevich isotherm.

Table 3
Isotherm model parameters for Mo(VI) adsorption to CCN at three temperatures

| Isotherm models | Expression formula | Parameters | 283.15 K | 293.15 K | 303.15 K |
|---|---|---|---|---|---|
| Langmuir | $\frac{C_e}{q_e}=\frac{C_e}{Q_0}+\frac{1}{Q_0 b}$ | $Q_0$ (mg g$^{-1}$) | 158.730 | 181.818 | 192.308 |
| | | $b$ (L mg$^{-1}$) | 0.058 | 0.116 | 0.219 |
| | | $R^2$ | 0.9977 | 0.9975 | 0.9986 |
| Freundlich | $\ln q_e=\frac{1}{n}\ln C_e+\ln k_F$ | $k_F$ (mg$^{1-n}$ L$^n$ g$^{-1}$) | 11.613 | 20.859 | 34.422 |
| | | $n$ | 2.002 | 2.334 | 2.865 |
| | | $R^2$ | 0.9361 | 0.9505 | 0.9743 |
| Temkin | $q_e=\frac{RT}{b_T}\ln A+\frac{RT}{b_T}\ln C_e$ | $A$ (L g$^{-1}$) | 1.948 | 6.110 | 37.745 |
| | | $b_T$ (kJ mol$^{-1}$) | 0.102 | 0.105 | 0.122 |
| | | $R^2$ | 0.9789 | 0.9715 | 0.9526 |
| Dubinin–Radushkevich | $\ln Q_e=\ln Q_m-\beta\varepsilon^2$ | $Q_m$ (mg g$^{-1}$) | 119.941 | 122.437 | 138.463 |
| | | β (mol$^2$ kJ$^{-1}$) | 1.603 | 0.601 | 0.330 |
| | | $E$ (kJ mol$^{-1}$) | 0.559 | 0.913 | 1.231 |
| | | $R^2$ | 0.9305 | 0.9031 | 0.9389 |

Table 4
Comparison of CCN and other adsorbents for Mo(VI) adsorption capacity

| Adsorbent | Adsorption capacity $Q_0$ (mg g$^{-1}$) | References |
|---|---|---|
| Chelating resin | 42.0 | [12] |
| Pyrite | 130.0 | [13] |
| Biochar modified by nanoscale zero-valent iron and cetyl-trimethyl ammonium bromide | 48.54 | [8] |
| Desulfurization steel slag | 4.38 | [14] |
| Nano-magnetic $CuFe_2O_4$ | 30.58 | [15] |
| Cetylpyridinium bromide-bentonite | 134.4 | [16] |
| Molybdate-imprinted chitosan/triethanolamine gel beads | 37.04 | [22] |
| Carminic acid modified anion exchanger | 13.5 | [34] |
| Hydrotalcite-like layered double hydroxides | 16.2 | [35] |
| Chitosan carbonization nanoparticle | 158.73–192.31 | This work |

while the physisorption process was reported to have adsorption energies less than –40 kJ mol$^{-1}$ [33]. The values of $b_T$ (0.102–0.122) obtained in the present study indicated that chemisorption and physisorption was involved in the adsorption process.

#### 3.2.4. Thermodynamic analysis

Temperature is a major influencing factor in the adsorption process. In this study, Mo(VI) adsorption on CCN was monitored at three different temperatures (283.15, 293.15, and 303.15 K) under optimized conditions by adapting the Khan and Singh [36] method. Thermodynamic parameters including changes in Gibbs free energy ($\Delta G°$), enthalpy ($\Delta H°$), and entropy ($\Delta S°$) are presented in Table 5. The negative values of $\Delta G°$ indicated that the adsorption process was spontaneous in nature. Besides, the decrease in negative value of $\Delta G°$ with the increase of temperature indicates that Mo(VI) adsorption process on CCN was more favorable at higher temperatures [37], which was mainly attributed to the higher temperature did not only enhance the free volume of CCN but also can get rid of the solvent molecules from the inter-facial region [38]. The values of $\Delta H°$ were positive in the process of Mo(VI) adsorbed on CCN, suggesting that the adsorption reaction was endothermic. The positive value of $\Delta S°$ suggested the increased randomness at the solid/solution interface during the adsorption of Mo(VI) on CCN.

### 3.3. Adsorption mechanism

#### 3.3.1. FTIR spectra

The adsorption pattern of metals onto materials is attributable to the active groups and bonds present on adsorption materials [39]. FTIR spectroscopy of CCN, before and after Mo(VI) binding, was used to determine which functional groups were responsible for Mo(VI) uptake. As shown in Fig. 7, the band at 3,425 cm$^{-1}$ is connected with the presence of –OH and –$NH_2$ stretching vibrations. The band at 1,622 cm$^{-1}$ corresponds to deformation modes of the N–H asymmetric stretching. After adsorbing Mo, some different adsorbance peaks and new peaks appeared in the FTIR spectra of CCN. The peak at wave number of 3,425 cm$^{-1}$ became

Table 5
Thermodynamic parameters for the adsorption of Mo(VI) on CCN

| Temperature (K) | $\Delta G°$ (kJ mol$^{-1}$) | $\Delta H°$ (kJ mol$^{-1}$) | $\Delta S°$ (J mol$^{-1}$ K$^{-1}$) | $R^2$ |
|---|---|---|---|---|
| 283.15 | –5.231 | | | |
| 293.15 | –7.437 | 54.285 | 210.303 | 0.9989 |
| 303.15 | –9.432 | | | |

weaker and shifted to a lower wave number (3,401 cm$^{-1}$), which might be due to the formation of hydrogen bonding between –OH and –$NH_2$ groups on CCN-Mo [19]. Another significant change was found at 1,622 cm$^{-1}$, the decreased wave number could be attributed to the formation of the coordinated –$NH_3^+$ and molybdate complexes. Besides, the presence of a narrow and weak peak at 901 cm$^{-1}$ might be due to asymmetric and symmetric stretching frequencies of Mo=O bond [40]. The new band at 651 cm$^{-1}$ of CCN-Mo was assigned to deformation modes of the Mo–O–Mo stretching vibration [41]. These results suggest that –OH and –$NH_2$ have participated in binding of molybdate anions onto the surface of CCN, which is similar to the adsorption of humic acid by magnetic chitosan nanoparticle [42].

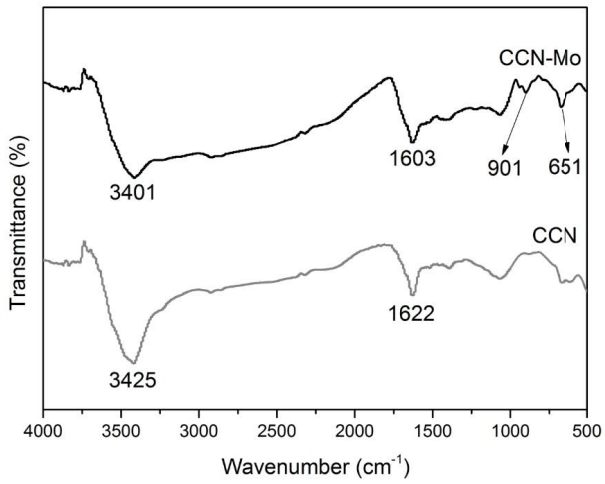


Fig. 7. FTIR spectra of CCN and CCN-Mo.

### 3.3.2. XPS spectra

XPS analysis was performed for further evidence the adsorption mechanism inferred by the FTIR analysis. As shown in Fig. 8, the characteristic peak of Mo appeared in XPS spectra of CCN-Mo. Moreover, the $3d_{3/2}$ and $3d_{5/2}$ spectra of Mo existed at 235.7 and 232.5 eV, respectively, were corresponded to the $Mo^{6+}$ state [43]. Obviously, there was no redox reaction occurred in the removal process of Mo(VI) adsorbed by CCN.

It was reported that the mechanism involving Mo(VI) adsorption is an electrostatic interaction process between protons and $MoO_4^{2-}$ in aqueous solution [3]. In this study, the adsorption of Mo(VI) was considerably influenced by the pH values of aqueous solution. From the Temkin isotherms,

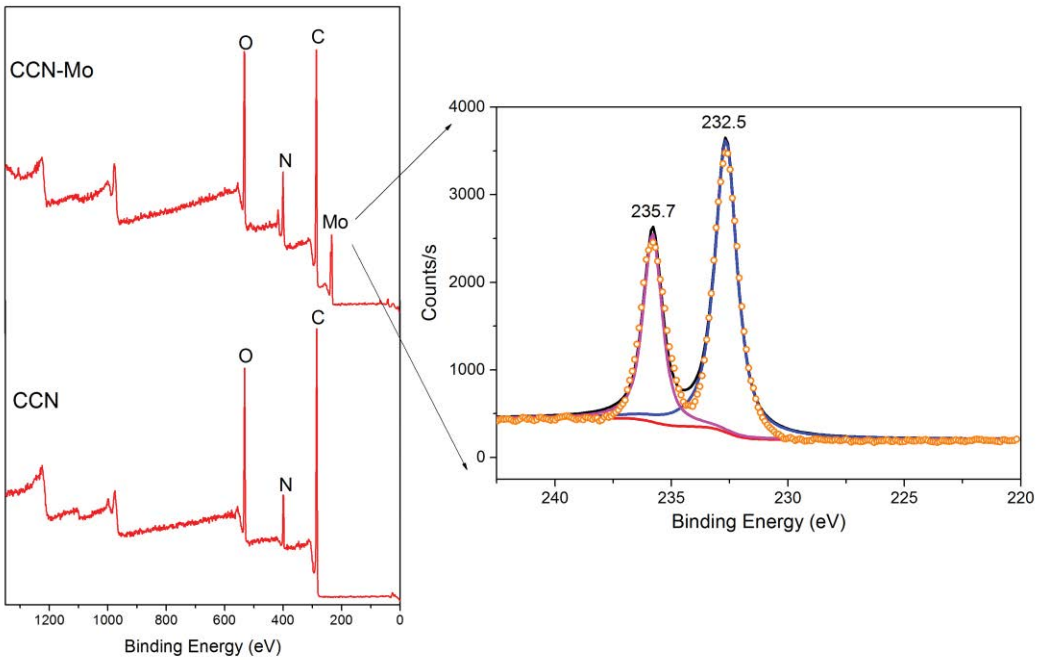


Fig. 8. XPS spectra of CCN and CCN-Mo.

typical bonding energy $b_T$ (0.102–0.122) indicated that the adsorption process seemed to be involved in the chemisorption and physisorption. According to FTIR results, –OH and $–NH_2$ participated in binding of molybdate anions onto the surface of CCN, which confirmed that hydrogen bonding played an important role in Mo adsorption. Besides, there was no redox reaction, because no evidence of low valence species of Mo was found in XPS analysis. Therefore, it was deduced that the main mechanisms of Mo(VI) adsorption on CCN should be controlled by electrostatic interaction (physisorption) and hydrogen bonding (chemisorption) mechanism.

### 3.4. Regeneration

The reusability is a crucial factor for designing an efficient adsorbent. A good adsorbent should have the advantage of a relatively high adsorption capacity and relatively high desorption efficiency which will reduce its economic cost. As shown in Fig. 3, little Mo(VI) was adsorbed onto when pH > 8, suggesting that alkaline solution could be used for the desorption of Mo(VI) from CCN-Mo. Therefore, 0.1 M NaOH solution was used for elution, which exhibited to be more available for desorption of Mo(VI) to the similar consistency principle and electrostatic repulsion [44]. Five successive cycles on adsorption/desorption were carried out in this study. As shown in Fig. 9, CCN showed good regeneration rate and the removal efficiency of CCN was still higher than 85% after regeneration for five times and the desorption rate also stayed around 83%. The slight decrease of the adsorption capacity may be attributed to the incomplete desorption, and the incomplete desorption of Mo(VI) may due to the dual process of physisorption and chemisorption [45]. The plausible mechanism for Mo(VI) removal and CCN regeneration is shown in Fig. 10.

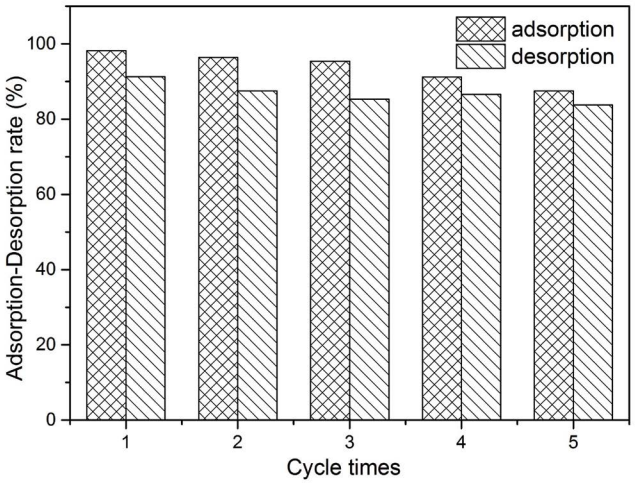


Fig. 9. Performance of CCN-Mo by multiple cycles of regeneration. Conditions: CCN dosage = 5.0 g $L^{-1}$, $T$ = 293.15 K, initial Mo concentration = 50 mg $L^{-1}$.

### 3.5. Real groundwater treatment

The adsorption/desorption experiment was also carried out by agitating 1.0 g of CCN with 100 mL groundwater containing 10 mg $L^{-1}$ Mo(VI) in a constant temperature oscillator. The results indicated that the adsorption/desorption rate could reach 78.20% and 75.44% after five successive cycles. Loss of Mo(VI) removal capacity compared with the static adsorption experiments was probably due to the competition of sulfate that existed in real groundwater [14]. It is suggested that CCN is a promising adsorbent for removing Mo(VI) from aqueous solution due to its potential practical applications in groundwater treatment.

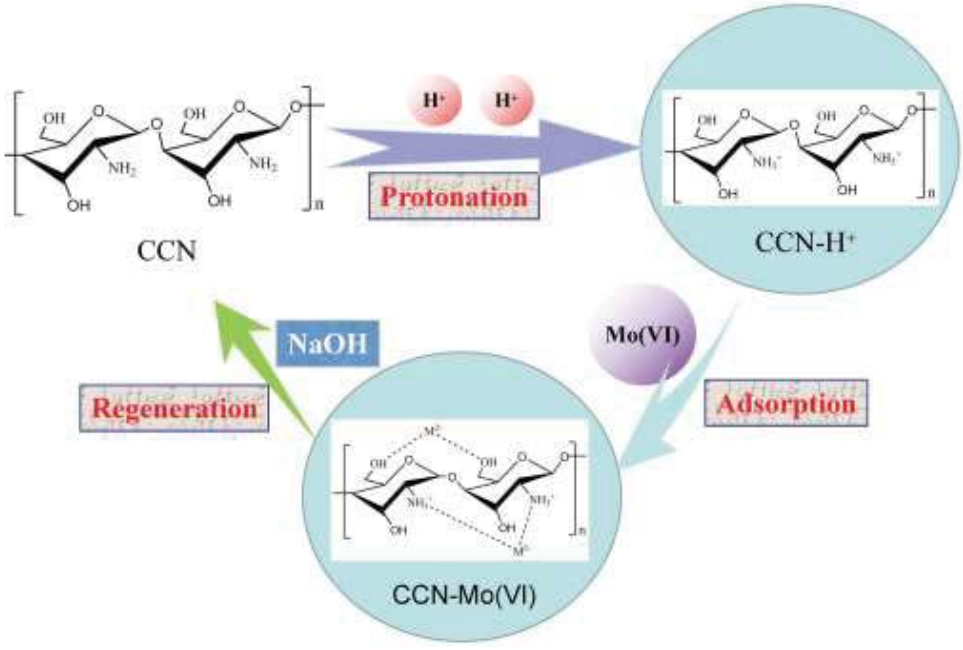


Fig. 10. Plausible mechanism for Mo(VI) removal and CCN regeneration. ($M^{2-}$ stands for $Mo_x^{VI}O_y^{2-}$).

## 4. Conclusions

The adsorbent studied in this paper is based on chitosan, which is a low-cost and biodegradable natural biopolymer. The effects of various conditions for Mo(VI) adsorption by CCN were investigated systematically. The experimental data could be well fitted by pseudo-second-order kinetic model and Langmuir isotherm model with the maximum monolayer adsorption capacity of 192.308 mg $g^{-1}$ at 303.15 K. Thermodynamic studies revealed that the adsorption of CCN with respect to Mo(VI) was a feasible, spontaneous and endothermic process. FTIR and XPS studies showed that electrostatic interaction and hydrogen bonding were the two major adsorption forces for the adsorption of Mo(VI) by CCN. On the basis of the low cost and easy availability of the raw material used for the preparation of CCN and its reasonably high adsorption/desorption capacity, CCN can be a potential candidate used for Mo(VI) removal from groundwater.

## Acknowledgments

This research was supported by the National Natural Science Foundation of China (51709001), the Natural Science Foundation of Anhui Province of China (1708085QD81), the Youth Foundation of Anhui University of Technology (QZ201520), and China Scholarship Council (201808340035). Constructive comments from anonymous reviewers are highly appreciated.

## References

[1] A. Afkhami, A.R. Norooz, Removal, preconcentration and determination of Mo(VI) from water and wastewater samples using maghemite nanoparticles, Colloids Surf., A, 346 (2009) 52–57.
[2] Y.J. Tu, T.S. Chan, H.W. Tu, S.L. Wang, C.F. You, C.K. Chang, Rapid and efficient removal/ recovery of molybdenum onto $ZnFe_2O_4$ nanoparticles, Chemosphere, 148 (2016) 452–458.
[3] C. Namasivayam, D. Sangeetha, Removal of molybdate from water by adsorption onto $ZnCl_2$ activated coir pith carbon, Bioresour. Technol., 97 (2006) 1194–1200.
[4] A. Moret, J. Rubio, Sulphate and molybdate ions uptake by chitin-based shrimp shells, Miner. Eng., 16 (2003) 715–722.
[5] P.L. Smedley, H.B. Nicolli, D.M.J. Macdonald, A.J. Barros, J.O. Tullio, Hydrogeochemistry of arsenic and other inorganic constituents in groundwaters from La Pampa, Argentina, Appl. Geochem., 17 (2002) 259–284.
[6] S. Das, M.J. Hendry, Adsorption of molybdate by synthetic hematite under alkaline conditions: effects of aging, Appl. Geochem., 28 (2013) 194–201.
[7] M.I.E. Halmi, H. Wasoh, S. Sukor, S.A. Ahmad, M.T. Yusof, M.Y. Shukor, Bioremoval of molybdenum from aqueous solution, Int. J. Agric. Biol., 16 (2014) 848–850.
[8] J.J. Lian, Y.G. Huang, B. Chen, S.S. Wang, P. Wang, S.P. Niu, Z.L. Liu, Removal of molybdenum(VI) from aqueous solutions using nano zero-valent iron supported on biochar enhanced by cetyl-trimethyl ammonium bromide: adsorption kinetic, isotherm and mechanism studies, Water Sci. Technol., 2017 (2018) 859–868.
[9] Y.C. Sun, J.Y. Yang, S.R. Tzeng, Rapid determination of molybdate in natural waters by coprecipitation and neutron activation analysis, Analyst, 124 (1999) 421–424.
[10] I. Polowczyl, P. Cyganowski, B.F. Urbano, B.L. Rivas, M. Bryjak, N. Kabay, Amberlite IRA-400 and IRA-743 chelating resins for the sorption and recovery of molybdenum(VI) and vanadium(V): equilibrium and kinetic studies, Hydrometallurgy, 169 (2017) 496–507.
[11] Z.N. Lou, J. Wang, X.D. Jin, L. Wan, Y. Wang, H. Chen, W.J. Shan, Y. Xiong, Brown algae based new sorption material for fractional recovery of molybdenum and rhenium from wastewater, Chem. Eng. J., 273 (2015) 231–239.
[12] S.H. Kalal, A.H. Panahi, N. Faramarzi, E. Moniri, A. Naeemy, H. Hoveidi, A. Abhari, A new chelating resin for preconcentration and determination of molybdenum by inductive couple plasma atomic emission spectroscopy, Int. J. Environ. Sci. Technol., 8 (2011) 501–512.
[13] B.C. Bostick, S. Fendorf, G.R. Helz, Differential adsorption of molybdate and tetrathiomolybdate on pyrite, Environ. Sci. Technol., 37 (2003) 285–291.
[14] J.J. Lian, S.G. Xu, N.B. Chang, C.W. Han, J.W. Liu, Removal of molybdenum(VI) from mine tailing effluents with the aid of loessial soil and slag waste, Environ. Eng. Sci., 30 (2013) 213–220.
[15] Y.J. Tu, C.F. You, C.K. Chang, T.S. Chan, S.H. Li, XANES evidence of molybdenum adsorption onto novel fabricated nano-magnetic $CuFe_2O_4$, Chem. Eng. J., 244 (2014) 343–349.
[16] A.A. Atia, Adsorption of chromate and molybdate by cetylpyridinium bentonite, Appl. Clay Sci., 41 (2008) 73–84.
[17] K. Li, P. Li, J. Cai, S. Xiao, H. Yang, A. Li, Efficient adsorption of both methyl orange and chromium from their aqueous mixtures using a quaternary ammonium salt modified chitosan magnetic composite adsorbent, Chemosphere, 154 (2016) 310–318.
[18] D. Kolodynska, Chitosan as an effective low-cost sorbent of heavy metal complexes with the polyaspartic acid, Chem. Eng. J., 173 (2011) 520–529.
[19] Q. Zhou, Q. Gao, W.J. Luo, C.J. Yan, Z.N. Ji, P. Duan, One-step synthesis of amino-functionalized attapulgite claynanoparticles adsorbent by hydrothermal carbonization of chitosan for removal of methylene blue from wastewater, Colloids Surf., A, 470 (2015) 248–257.
[20] G. Crini, P.M. Badot, Application of chitosan, a natural aminopolysaccharide, for dye removal from aqueous solutions by adsorption processes using batch studies: a review of recent literature, Prog. Polym. Sci., 33 (2008) 399–447.
[21] K.Z. Elwakeel, A.A. Atia, A.M. Donia, Removal of Mo(VI) as oxoanions from aqueous solutions using chemically modified magnetic chitosan resins, Hydrometallurgy, 97 (2009) 21–28.
[22] L. Zhang, J.Q. Xue, X.W. Zhou, X. Fei, Y. Wang, Y.Z. Zhou, L.L. Zhong, X.L. Han, Adsorption of molybdate on molybdate-imprinted chitosan/triethanolamine gel beads, Carbohydr. Polym., 114 (2014) 514–520.
[23] F.A. Bertoni, A.C. Medeot, J.C. Gonzalez, L.F. Sala, S.E. Bellu, Application of green seaweed biomass for $Mo^{VI}$ sorption from contaminated waters. Kinetic, thermodynamic and continuous sorption studies, J. Colloid Interface Sci., 446 (2015) 122–132.
[24] SEPA, Water and Exhausted Water Monitoring Analysis Method, 4th ed., Environmental Science Press, China, 2002.
[25] J.C. Andrade, C.J. Cuelbas, S.P. Eiras, Spectrophotometric determination of Mo(VI) in steel using a homogeneous ternary solvent system after single-phase extraction, Talanta, 47 (1998) 719–727.
[26] W.S.W. Ngah, L.C. Teong, R.H. Toh, M. Hanafiah, Comparative study on adsorption and desorption of Cu(II) ions by three types of chitosan-zeolitecomposites, Chem. Eng. J., 223 (2013) 231–238.
[27] Q.P. Kong, J.Y. Wei, Y. Hu, C.H. Wei, Fabrication of terminal amino hyperbranched polymer modified graphene oxide and its prominent adsorption performance towards Cr(VI), J. Hazard. Mater., 363 (2019) 161–169.
[28] Y. Xiong, C.B. Chen, X.J. Gu, B.K. Biswas, W.J. Shan, Z.N. Lou, D.W. Fang, S.L. Zang, Investigation on the removal of Mo(VI) from Mo-Re containing wastewater by chemically modified persimmon residua, Bioresour. Technol., 102 (2011) 6857–6862.
[29] W.J. Shan, Y.N. Shu, H. Chen, D.Y. Zhang, W. Wang, H.Q. Ru, Y. Xiong, The recovery of molybdenum(VI) from rhenium(VII) on amino-functionalized mesoporous materials, Hydrometallurgy, 165 (2016) 251–260.
[30] S. Debnath, U.C. Ghosh, Nanostructured hydrous titanium (IV) oxide: synthesis, characterization and Ni(II) adsorption behavior, Chem. Eng. J., 152 (2009) 480–491.

[31] W.J. Weber, J.C. Morris, Kinetics of adsorption on carbon from solution, J. Sanit. Eng. Div., 89 (1963) 31–60.
[32] A. Mittal, A. Malviya, D. Kaur, J. Mittal, L. Kurup, Studies on the adsorption kinetics and isotherms for the removal and recovery of Methyl Orange from wastewaters using waste materials, J. Hazard. Mater., 148 (2007) 229–240.
[33] F. Helfferich, Ion Exchange, McGraw-Hill, New York, USA, 1962.
[34] M.M. EI-Moselhy, A.K. Sengupta, R. Smith, Carminic acid modified anion exchanger for the removal and preconcentration of Mo(VI) from wastewater, J. Hazard. Mater., 185 (2011) 442–446.
[35] S. Paikaray, M.J. Hendry, J. Essilfie-Dughan, Controls on arsenate, molybdate, and selenate uptake by hydrotalcite-like layered double hydroxides, Chem. Geol., 345 (2013) 130–138.
[36] A.A. Khan, R. Singh, Adsorption thermodynamics of carbofuran on Sn(IV) arsenosilicate in $H^+$, $Na^+$ and $Ca^{2+}$ forms, Colloids Surf., 24 (1987) 33–42.
[37] S.G. Wang, X.W. Liu, W.X. Gong, W. Nie, B.Y. Gao, Q.Y. Yue, Adsorption offulvic acids from aqueous solutions by carbon nanotubes, J. Chem. Technol. Biotechnol., 82 (2007) 698–704.
[38] S. Wang, Y.Y. Zhai, Q. Gao, W.J. Luo, H. Xia, C.G. Zhou, Highly efficient removal of acid red 18 from aqueous solution by magnetically retrievable chitosan/carbon nanotube: batch study, isotherms, kinetics, and thermodynamics, J. Chem. Eng. Data, 59 (2013) 39–51.
[39] K.K. Krishnani, M.X. Xiaoguang, C. Christodoulatos, V.M. Boddu, Biosorption mechanism of nine different heavy metals onto biomatrix from rice husk, J. Hazard. Mater., 153 (2008) 1222–1234.
[40] M. Iqbal, A. Saeeda, S.I. Zafarb, FTIR spectrophotometry, kinetics and adsorption isotherms modeling, ion exchange, and EDX analysis for understanding the mechanism of $Cd^{2+}$ and $Pb^{2+}$ removal by mango peel waste, J. Hazard. Mater., 164 (2009) 161–171.
[41] F. Mauge, J.P. Gallas, J.C. Lavalley, G. Busca, G. Ramis, V. Lorenzelli, FT-IR and FT-FIR studies of vanadium, molybdenum and tungsten oxides supported on different carriers, Microchim. Acta, 95 (1988) 57–61.
[42] C.L. Dong, W. Chen, C. Liu, Y. Liu, H.C. Liu, Synthesis of magnetic chitosan nanoparticle and its adsorption property for humic acid from aqueous solution, Colloids Surf., A, 446 (2014) 179–189.
[43] E. Yavuz, K.V. Ozdokur, I. Cakar, S. Kocak, F.N. Ertas, Electrochemical preparation, characterization of molybdenum-oxide/platinum binary catalysts and its application to oxygen reduction reaction in weakly acidic medium, Electrochim. Acta, 151 (2015) 72–80.
[44] J. Li, Q. Zhang, J. Feng, W. Yan, Synthesis of PPy-modified $TiO_2$ composite in $H_2SO_4$ solution and its novel adsorption characteristics for organic dyes, Chem. Eng. J., 225 (2013) 766–775.
[45] C.Y. Chen, J.C. Chang, A.H. Chen, Competitive biosorption of azo dyes from aqueous solution on the templated crosslinked-chitosan nanoparticles, J. Hazard. Mater., 185 (2011) 430–441.